ELSEVIER

Journal of Nuclear Materials 241–243 (1997) 199–213

journal of nuclear materials

Classical drifts in the tokamak SOL and divertor: models and experiment

A.V. Chankin *

JET Joint Undertaking, Abingdon, Oxfordshire OX14 3EA, UK

Abstract

Classical drifts offer potential explanations for a variety of physical phenomena such as poloidal asymmetries, possible extra pinch or outward flow of plasma depending on the B_t direction, non-ambipolarity of radial plasma flow and current flow towards the target. Their incorporation into 2D numerical codes is promising to greatly improve their predictive capacity. The paper contains basic analysis of drift and fluid flows, modified boundary conditions, ad-hoc models and summary of experimental results which are widely regarded as having their origin in drift motions. Unresolved issues of plasma transport are highlighted.

Keywords: Poloidal divertor; SOL plasma; Divertor plasma; Analytical model

1. Introduction

Guiding center drifts can significantly influence distribution of plasma parameters over the magnetic surface, radial, poloidal and toroidal plasma flows, perpendicular electric conductivity, etc. Simple estimates (Section 2.1) show that drifts' relative contribution to both radial and poloidal transport of particles scales as the ratio of ion poloidal Larmor radius, calculated for ion sound speed, $\rho_{s\theta} = c_s/\omega_{i\theta}$, to the radial decay length of plasma parameters. This ratio is often of the order of unity in the tokamak SOL.

The importance of drifts in the edge transport has demanded their inclusion in two-dimensional codes (see, for exampl, Refs. [1–3]). Recent developments in this area were reviewed in Ref. [4]. The present paper focuses on basic analysis of drift and fluid flows, boundary conditions in the presence of drifts, ad-hoc models and experimental results which are widely regarded as being (at least partly) caused by the drifts. Qualitative understanding of the phenomena, obtained from simple models, is essential for both general understanding of the SOL behavior and code development. Throughout the paper, a single null X-point divertor configuration is assumed. For simplicity, formulae are written in the form which assumes the right angle between the poloidal projection of the magnetic separatrixes and the surface of the divertor target.

2. Drift flows in the tokamak edge

2.1. Main drift motions; fluid and guiding center approximations

The main guiding center drifts are depicted on Fig. 1 for the case of 'normal' toroidal field (B_t) direction, when the ion $\mathbf{B} \times \nabla B$ drift is directed towards the X-point. The direction of all the drifts is reversed for the opposite B_t direction. The direction of the plasma current, which is assumed to be parallel to the toroidal field on Fig. 1 (the helicity of field lines is indicated by the segment of the field line near the outer side), does not affect any equations. Since the fluid approximation, based on momentum conservation equations, is more universal and is more often used in models and numerical codes, it seems appropriate here to demonstrate the relationship between the fluid and guiding center flows.

The momentum conservation equation reads [5]

$$\frac{\partial}{\partial t}(nm\mathbf{V}) + \nabla\left(nm\mathbf{V}\mathbf{V}\overleftrightarrow{p}\right) = en(\mathbf{E} + \mathbf{V} \times \mathbf{B}) + \mathrm{R}. \quad (1)$$

* Permanent address: Russian Scientific Center 'Kurchatov Institute', Institute for Nuclear Fusion, Moscow, Russia.

PII S0022-3115(96)00505-3

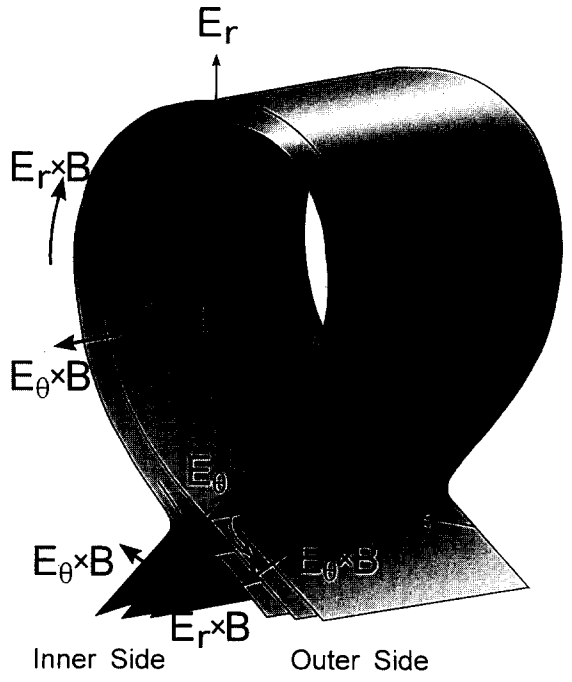

Fig. 1. Schematic illustration of the main guiding center drifts for the case of normal toroidal field (B_t) direction (ion $\mathbf{B}\times\nabla B$ drift is directed towards the X-point). The direction of all the drifts is reversed for the reversed B_t direction.

In this and the following equations of this section the electric charge e is assumed to be positive for ions and negative for electrons. $\mathbf{R}$ is the friction force exerted on particles of a specified type by another and $\overleftrightarrow{p}$ is the pressure tensor. The pressure tensor can be written in the form [6]

$$\overleftrightarrow{p} = p_{\|}\mathbf{BB}/B^2 + p_{\perp}\left(\overleftrightarrow{\delta} - \mathbf{BB}/B^2\right). \tag{2}$$

Here $\delta^{\leftrightarrow}$ is a unit tensor. Perpendicular velocity $\mathbf{V}_{\perp} \equiv \mathbf{V} - \mathbf{B}(\mathbf{V}\cdot\mathbf{B})/B^2$ can be extracted from the term $\mathbf{V}\times\mathbf{B}$ of Eq. (1) by vector multiplying it by $\mathbf{B}$ and using formulae of tensor analysis to open $\nabla(nm\mathbf{VV} + \mathrm{p}^{\leftrightarrow})$. By adding parallel flux density $nV_{\|}\cdot\mathbf{B}/B$ to the perpendicular one and neglecting cross products $nm\mathbf{V}_{\|}\mathbf{V}_{\perp}$ of the tensor (they will not change the result substantially), the total flux density for steady state conditions ($\partial/\partial t = 0$) can thus be obtained:

$$n\mathbf{V} = nV_{\|}\frac{\mathbf{B}}{B} + \frac{n}{B^2}\mathbf{E}\times\mathbf{B} + \frac{1}{eB^2}\mathbf{R}\times\mathbf{B} + \frac{1}{eB^2}\mathbf{B}\times\nabla p_{\perp} + \frac{\left(p_{\|} - p_{\perp} + nmV_{\|}^2\right)}{eB^3}\mathbf{B}\times\mathbf{B}\cdot\nabla\left(\frac{\mathbf{B}}{B}\right). \tag{3}$$

The last term in this equation is often ignored in the models. It cannot, however, be neglected in the SOL, where even for isotropic pressure, $p_{\|} = p_{\perp}$, the term with $nmV_{\|}^2$ can make a significant contribution to the ion radial flux, comparable to the radial component of the $\mathbf{B}\times\nabla p_{\perp}$ flux.

The notion of drift guiding center flux only makes sense in a quasi homogeneous plasma, where magnetic field components and plasma parameters do not vary substantially on the scale of the ion Larmor radius. The charged particle distribution function can then be expanded into fast rotations of Larmor circles and averaged guiding center drift (see, for example, Ref. [5] and references therein). The flux due to the superposition of Larmor circle rotations is given by the so called magnetization flux $curl\mathbf{K}$, where $\mathbf{K} = -(p_{\perp}/eB^2)\mathbf{B}$. Total (fluid) particle flux density can be represented as

$$n\mathbf{V} = n\langle\mathbf{v}_{\mathrm{dr}}\rangle + curl\mathbf{K} + n\mathbf{V}_{\mathrm{coll}}. \tag{4}$$

Here, $\mathbf{v}_{\mathrm{dr}}$ is the drift velocity of a Larmor guiding center and $\langle\ldots\rangle$ denotes averaging over the distribution function; $n\mathbf{V}_{\mathrm{coll}}$ gives particle flux due to electron–ion collisions equal to $\mathbf{R}\times\mathbf{B}/eb^2$ — the third term on the rhs of Eq. (3). This form of the total particle flux clearly shows that, apart from the guiding center contribution, $n\langle\mathbf{v}_{\mathrm{dr}}\rangle$ and Coulomb collisions, the remainder of the particle flux is automatically divergence-free as *curl* of a vector. In many cases, where only accumulation or sink of particles or energy in space is of interest, it may be more convenient to treat the plasma as an ensemble of Larmor guiding centers. It may also be of benefit in numerical calculations on finite mesh, since the part of the flux which has to be made divergence-free, $curl\mathbf{K}$, is much greater than $n\langle\mathbf{v}_{\mathrm{dr}}\rangle$ thereby causing problems of accumulating errors in the numerical scheme. Elimination of divergence-free terms from the numerical scheme was used as a basis for implementation of drifts into the EDGE2D code at JET [3].

An expression for the drift velocity of an individual particle can be found in [5]. Its integration over the distribution function gives

$$n\langle\mathbf{v}_{\mathrm{dr}}\rangle = n\langle\mathrm{v}_{\mathrm{dr}\|}\rangle\frac{\mathbf{B}}{B} + \frac{n}{B^2}\mathbf{E}\times\mathbf{B} + \frac{p_{\perp}}{eB^3}\mathbf{B}\times\nabla B + \frac{\left(p_{\|} + nmV_{\|}^2\right)}{eB^3}\mathbf{B}\times\mathbf{B}\cdot\nabla\left(\frac{\mathbf{B}}{B}\right) + \frac{p_{\perp}}{eB^3}\mathbf{B}\left(\mathbf{B}\cdot curl\left(\frac{\mathbf{B}}{B}\right)\right). \tag{5}$$

The second term on the right hand side of this equation describes the $\mathbf{E}\times\mathbf{B}$ drift, poloidal and radial components of which are shown on Fig. 1, the third term $-\mathbf{B}\times\nabla B$ (or simply ∇B) almost vertical drift with its direction for ions shown on Fig. 1 (for the electrons it has an opposite direction), the fourth term is the curvature drift, which is also almost vertical and is approximately in the same direction as the ∇B drift. The last term makes a small correction to the parallel guiding center flux which is offset by parallel component of $curl\mathbf{K}$.

Depending on whether the particle flux is considered according to Eq. (3), or according to Eq. (5) with Eq. (4) implied, the plasma is treated in fluid or guiding center approximations. As one can see, the main difference between the two approaches (apart from the term with ion–electron friction, missing in Eq. (5), which could, however, be easily added by virtue of the fact that Coulomb collisions are predominantly distant and only slightly disturb the Larmor orbit) is that the fluid form (Eq. (3)) explicitly contains a large pressure gradient term: the diamagnetic flux $\mathbf{B}\times\nabla p_\perp/eB^2$. All other terms with pressure in both Eqs. (3) and (5) are much smaller, only of the order of λ_p/R of the diamagnetic flux, where λ_p is the pressure decay length and R – major radius. In the literature the diamagnetic flux is often called the diamagnetic drift. This flux, however, is almost entirely dominated by the magnetization flux, $curl\mathbf{K}$ and should not be confused with any guiding center drift. The difference between these two fluxes, $(\mathbf{B}\times\nabla p_\perp/eB^2 - curl\mathbf{K})$, is of the order of λ_p/R of each of them individually. The non-divergence-free part of the diamagnetic flux cannot, of course, be totally ignored. It is of the same order as the ∇B and curvature drifts and is responsible for generation of Pfirsh–Schlüter currents (Section 5.1). Their origin and spatial distribution in the SOL and divertor has recently been studied by Schaffer et al. [7].

Equivalence between the two approximations can be verified by substituting $n\langle\mathbf{v}_{dr}\rangle$ from Eq. (5) and an expression for the magnetization flux:

$$curl\mathbf{K} = \frac{\mathbf{B}\times\nabla p_\perp}{eB^2} - \frac{2p_\perp}{eB^3}\mathbf{B}\times\nabla B - \frac{p_\perp}{eB^2}curl\mathbf{B}, \qquad (6)$$

into Eq. (4). Then, with the help of the vector formula: $\mathbf{B}\times\nabla\mathbf{B} + Bcurl\mathbf{B} - \mathbf{B}(\mathbf{B}\cdot curl(\mathbf{B}/B)) = \mathbf{B}\times\mathbf{B}\cdot\nabla(\mathbf{B}/B)$, Eq. (4) takes exactly the form of Eq. (3).

Similar equivalence exists between fluid and drift energy fluxes ([5], p. 262). If collisions are neglected (this includes parallel collisional heat conduction), then the total energy flux can be written both as a sum of fluid convective and heat fluxes:

$$\mathbf{q} = \frac{5}{2}nT\mathbf{V} + \frac{5}{2}\frac{nT}{eB^2}\mathbf{B}\times\nabla T, \qquad (7)$$

and as a sum of guiding center convective flux and a *curl* of a vector:

$$\mathbf{q} = \frac{5}{2}nT\langle\mathbf{v}_{dr}\rangle - curl\left(\frac{5}{2}\frac{nT^2}{eB^2}\mathbf{B}\right). \qquad (8)$$

2.2. The contribution of drifts to edge transport

If the difference between ion and electron temperatures is ignored, poloidal fluxes for both diamagnetic and $\mathbf{E}\times\mathbf{B}$ drifts can be estimated as: $\Gamma_\theta^{dr}\approx p/eB\lambda_{SOL}$. Parallel flow with the ion sound speed causes poloidal flux: $\Gamma_\theta^{\parallel}\approx nc_sB_\theta/B$. By replacing pressure with $nm_ic_s^2$, the ratio of the two fluxes can be expressed as

$$\Gamma_\theta^{dr}/\Gamma_\theta^{\parallel}\approx\rho_{s\theta}/\lambda_{SOL}, \qquad (9)$$

where $\rho_{s\theta}=c_s/\omega_{i\theta}$ and $\omega_{i\theta}=eB_\theta/m_i$ – ion poloidal gyro frequency.

The same scaling can be deduced for the ratio of radial components of diamagnetic and $\mathbf{E}\times\mathbf{B}$ drift fluxes to the anomalous radial transport in the scrape-off layer [8]. Radial flux due to the diamagnetic and $\mathbf{E}\times\mathbf{B}$ drifts can roughly be estimated as $\Gamma_r^{dr}\approx p/eBa$, where minor radius a serves as a characteristic length of poloidal variation of plasma pressure in the SOL. Radial anomalous particle flux is $\Gamma_r^{an}\approx nD_\perp/\lambda_{SOL}$. By employing standard expression for the SOL width: $\lambda_{SOL}\approx\sqrt{D_\perp qR/c_s}$ (see, for example, Ref. [9]), their ratio can also be expressed as in Eq. (9):

$$\Gamma_r^{dr}/\Gamma_r^{an}\approx\rho_{s\theta}/\lambda_{SOL}. \qquad (10)$$

Since this ratio is typically of the order of unity in the scrape-off layer, drift fluxes can strongly affect the overall flux pattern in this region.

According to the above scaling, one should expect a smaller drift contribution to the plasma transport in low power high density discharges, which have low temperature throughout the SOL and divertor. As a function of plasma temperature and radial diffusion coefficient, the $\rho_{s\theta}/\lambda_{SOL}$ ratio scales as $T^{3/4}D_\perp^{-1/2}$ (a relation $\lambda_{SOL}\approx\sqrt{D_\perp qR/c_s}$ is implied here) and a very steep dependence of $D_\perp$ on T is needed to offset the effect of the $T^{3/4}$ dependence. Experimentally found dependence of $D_\perp$ on T is consistent with the scaling $D_\perp\sim T^\alpha$, where $\alpha=0$–1 [10,11]. Ionization of neutrals in the scrape-off layer at high density (low temperature) provides an additional widening of the SOL, further reducing the $\rho_{s\theta}/\lambda_{SOL}$ ratio. In the experiment, the scrape-off layer usually gets wider in high density discharges.

On the other hand, even during the plasma detachment from the target, drift contributions should make a significant impact on plasma behavior in the main SOL provided it is sufficiently 'hot' and large poloidal variation of electron temperature exists which gives rise to, for example, radial $\mathbf{E}\times\mathbf{B}$ drift. So far conditions with 'hot' SOL plasma and detachment from the target have not been realized in the experiment [12].

3. Boundary conditions at the target in the presence of drifts

In the absence of drifts, according to Chodura [13] and Riemann [14] the ion parallel flow reaches or exceeds the ion speed at the entrance to the magnetic pre-sheath layer (mps). This criterion is deduced from the requirement of smooth non-oscillating potential drop towards the surface

of the target and represents an extension of the Bohm criterion [15] for the case of magnetic field oblique to the surface.

In the presence of poloidal $\mathbf{E}\times\mathbf{B}$ drift the boundary condition on the minimal parallel velocity at the mps entrance is modified. Stangeby and Chankin [16] and Hutchinson[17] have shown that it is the combined effect of the $\mathbf{E}\times\mathbf{B}$ drift velocity and parallel velocity with which ions approach the surface that has to achieve a certain minimal value to ensure a smooth transition of electric potential through the mps and the Debye sheath. For the simplest case of flux surfaces perpendicular to the material surface in the poloidal cross-section, the approximate form of the boundary condition on the minimal (in absolute value) Mach number of parallel plasma flow (the complete form of the criterion derived in [16] is too cumbersome to present here), which only includes the effect of the poloidal $\mathbf{E}\times\mathbf{B}$ drift is

$$\begin{cases} M_{\rm in} = 1 - M_{E,\rm in} \\ M_{\rm out} = -1 - M_{E,\rm out} \end{cases} \tag{11}$$

for inner and outer targets. Here $M = V_{\|}/c_{\rm s}$, $M_E = \pm E_{\rm r}/B_\theta c_{\rm s}$ and it is assumed that positive velocities (both parallel and perpendicular) are directed from the outer to the inner side (see $V_{\|}$ in Fig. 1). Therefore, the sign of M_E is negative for normal $B_{\rm t}$ direction (poloidal $\mathbf{E}\times\mathbf{B}$ drift is directed towards the outer target) and positive for reversed $B_{\rm t}$ direction. The parallel ion velocity has to be adjusted to compensate for the velocity of the poloidal $\mathbf{E}\times\mathbf{B}$ drift towards/away from the target, so that the total velocity with which ions approach the surface would be equal to $c_{\rm s}\cdot B_\theta/B$, unless there are specific reasons why this velocity should be even higher in absolute value (such as the onset of a free-standing sonic transition some distance away from the target). The above boundary condition has also been used by Cohen and Ryutov [18].

According to Eq. (11), the poloidal diamagnetic flux does not affect the boundary condition on the minimal parallel ion velocity. This is because the diamagnetic flux is almost divergence-free, as was demonstrated in Section 2.1. Moreover, this conclusion can even be extended to the mps layer, where drift approximation is not valid, as was shown by Chankin and Stangeby [19]. What happens then to the poloidal diamagnetic flows when they come closer to the target? After reaching the entrance to the mps, the diamagnetic flows cross through the magnetic pre-sheath in the direction normal to the magnetic surfaces and then continue 'poloidally' on private magnetic surfaces [19]. The neglect of the diamagnetic flux in the boundary condition has, however, recently been disputed by Claaßen and Gerhauser [20,21].

In numerical codes the criterion on the minimal ion velocity is often imposed on the total *poloidal* ion velocity before the mps entrance. The contribution from the ion poloidal diamagnetic flux then must be included, keeping in mind, of course, that it does not reach the target but, after entering the mps, is diverted along the target surface. The boundary condition then takes the form

$$V_{{\rm i}\theta} = \frac{B_\theta}{B} M c_{\rm s} + \frac{B_\varphi}{enB^2}\nabla_{\rm r} p_{\rm i}. \tag{12}$$

Cohen and Ryutov [22] considered the boundary condition for the current density towards the target and their conclusion is essentially that the relation between the parallel current density and potential drop across the magnetic pre-sheath and the Debye sheath is unaffected by the drifts:

$$j_{\|} = enc_{\rm s}\left[1 - \exp\left(e(\Phi - \Phi_{\rm f})/T_e\right)\right]. \tag{13}$$

Here Φ is the potential before the mps entrance and $\Phi_{\rm f}$ is the floating potential (see, for example, Ref. [9]). Again, for the *poloidal* component of the current density at the mps entrance, one should correct for the diamagnetic current density:

$$j_\theta = \frac{B_\theta}{B} enc_{\rm s}\left[1 - \exp\left(-\frac{e(\Phi - \Phi_{\rm f})}{T_e}\right)\right] + \frac{B_\varphi}{B^2}\nabla_{\rm r} p. \tag{14}$$

Boundary conditions for the parallel energy flux at the mps look very similar to the ones in the absence of drifts (see, for example, Ref. [23]) and are formulated in [3]:

$$\tfrac{5}{2} p_\alpha M c_{\rm s} + q_{\|} = \beta p_\alpha M c_{\rm s}. \tag{15}$$

Here $q_{\|} = k_{\alpha\|}\nabla_{\|}T_\alpha$ is the parallel heat flux density of species α. Coefficient β is $\approx 5/2$ for ions and $(2 + e\Phi/T_{\rm e})$ for electrons.

4. Experiments with toroidal field reversal: Explanation of in–out asymmetries through the influence of drifts

The direction of the toroidal field determines the direction of drift flows. It is therefore widely accepted that poloidal asymmetries in the SOL, which are sensitive to the field direction, are caused by the drifts.

4.1. Summary of experimental observations

The average shift in the asymmetries, independent of the field direction, is for denser and colder plasma at the inner target. The temperature asymmetry in favour of the outer target is explained by higher total power flow through the outboard part of the magnetic surface [24]. This is generally attributed to the geometrical toroidal effect of the surplus of its area over the innerboard one. The Shafranov shift and poloidal asymmetry in anomalous heat transport in favour of the outer side [25] may also contribute to the temperature assymetry. As pressure $p_{\rm e} = n_{\rm e}T_{\rm e}$ tends to reach equilibrium along the field lines: $p_{\rm e}^{\rm in} = p_{\rm e}^{\rm out} = p_{\rm e}$, higher density ($n_{\rm e}^{\rm in} = p_{\rm e}/T_{\rm e}^{\rm in}$) is achieved at the inner

target, while higher power ($p_{target}^{out} \sim n_e^{out}(T_e^{out})^{3/2}$) ~ $p_e(T_e^{out})^{1/2}$) flows towards the outer target.

The effect of the toroidal field direction on the power asymmetries, as seen in experiment, is the following. Excessive power load to the outer strike zone is usually observed in the 'normal' toroidal field direction (ion ∇B drift directed towards the target in single null X-point discharges), whereas for the 'reversed' toroidal field (ion ∇B drift is directed away from the target) power sharing between the targets is much more symmetric [26–35,8]. This tendency is illustrated by Fig. 2, representing results on power to the target and radiated power in–out asymmetries in JT-60U obtained by Asakura et al. [30]. At medium and high densities the total power flowing to the outer divertor branch ($P_{target} + P_{rad,div}$), after the local strike radiation is taken into account, is slightly larger than that to the inner divertor branch. Such a nearly equal balancing of the total power sharing between the two divertor branches is not a universal case, however, and can vary depending on the machine/regime parameters. More symmetric heat load to the target in reversed B_t discharges at medium and high densities is explained by the asymmetry in the radiated power, which is inboard dominated in the normal and outboard dominated — in the reversed B_t plasmas. Possible explanations for inboard dominated

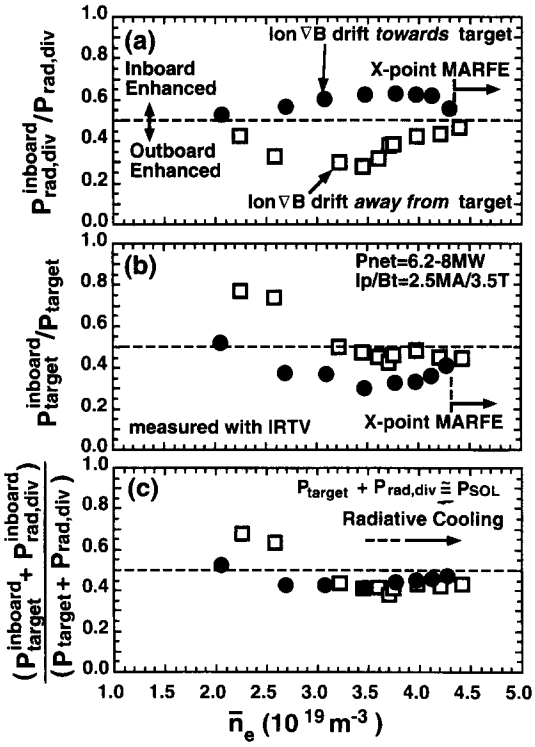

Fig. 2. Fractions of (a) radiation power loss, (b) heat load and (c) total loss of power in the inboard divertor for normal and reversed B_t directions in JT-60U as a function of $\bar{n}_e$ at safety factor $q_{eff} = 3.5$.

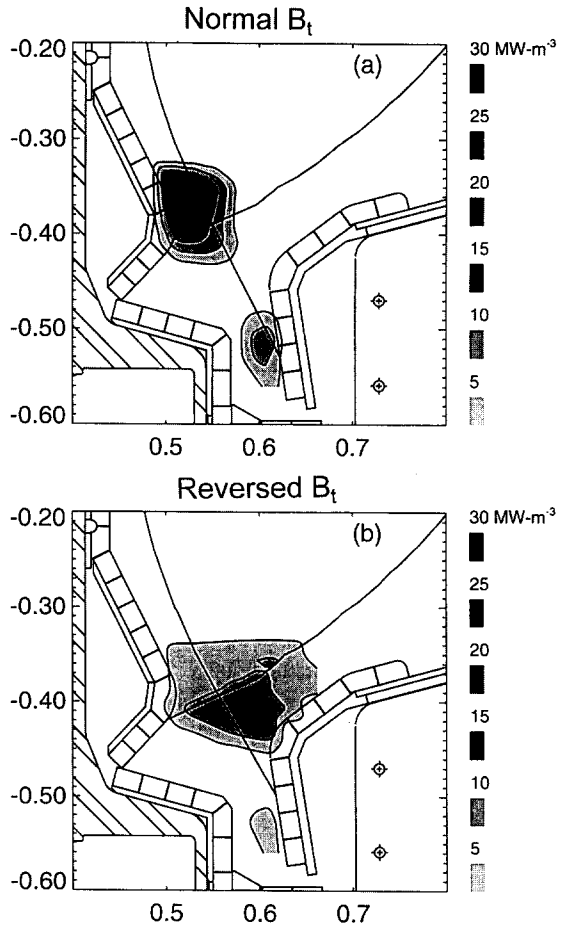

Fig. 3. Tomographic reconstruction of radiative power loss for moderate density plasma ($\bar{n}_e = 1 \times 10^{20}$ m^{-3}) in Alcator C-Mod for normal (a) and reversed (b) B_t direction.

P_{target} at low $\bar{n}_e$ in reversed B_t case will be discussed in Section 4.2. Power to the target and radiated power asymmetries are substantially suppressed at very high densities.

Asymmetries in plasma parameters at the target in the field reversal experiments were studied in Refs. [35–41,8]. Ref. [35] by Hutchinson et al. provides a good illustration of tomographic reconstruction of the radiative power in Alcator C-Mod. Fig. 3, replicated from this Ref., shows radiative loss pattern in Ohmic discharges for the two field configurations at $\bar{n}_e = 1 \times 10^{20}$ m^{-3}, which is a medium density for this machine. The normal field plasma is dominated by radiation from the inner divertor, while for the reversed field plasma the radiation zone is shifted towards the outer divertor. Langmuir probe measurements and the D_α emission revealed much denser and cooler plasma at the inner side with higher recycling of neutrals there. The sign of n_e and T_e asymmetries changed following the field reversal, but the averaged shift in the asymmetries, independent of the field direction, was for denser and colder plasma at the inner side, as expected. For

higher density, the effects of the field reversal were found to be much less dramatic.

A dedicated series of L-mode discharges with both B_t directions and a wide variation of the toroidal field and plasma current has been performed in JET [42,38,8]. The results are broadly consistent with those obtained from other machines. In/out ratios of radiated power, H_α emission and peak ion saturation current density as a function of q_{95} are shown in Fig. 4 [8]. The field reversal has largely eliminated strong asymmetries in these parameters and the distribution of H_α, and P_{rad} has become slightly shifted to the outer side. Fig. 5 [8] demonstrates profiles of j_{sat}, T_e and n_e obtained by target Langmuir probes during the diagnostic radial sweep of the X-point for the pair of discharges with $q_{95} = 3.6$. More symmetry is achieved in the plasma parameters distribution between the targets in the reversed field plasmas due to shifts in n_e and T_e distributions in the opposite direction: n_e from the inner to the outer side and T_e from the outer to the inner side. These shifts in plasma parameters have been previously identified as the most robust features of field reversal [36].

At very high densities, closer to the plasma detachment from the targets, the formation of a MARFE state, or density limit disruption, the B_t reversal has much weaker affect on all the divertor asymmetries (see, for example, Refs. [8,35,41]), however, the detachment density operation window is narrower in reversed field plasmas [43,44].

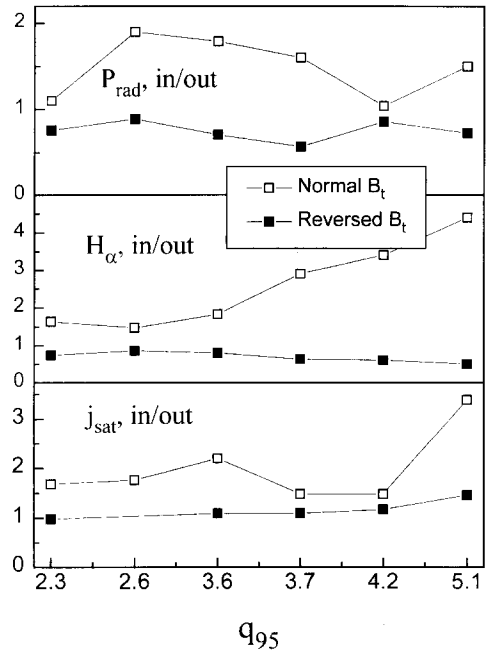

Fig. 4. q-dependence of in–out asymmetries in local radiated power, H_α intensity and peak ion saturation current density in JET.

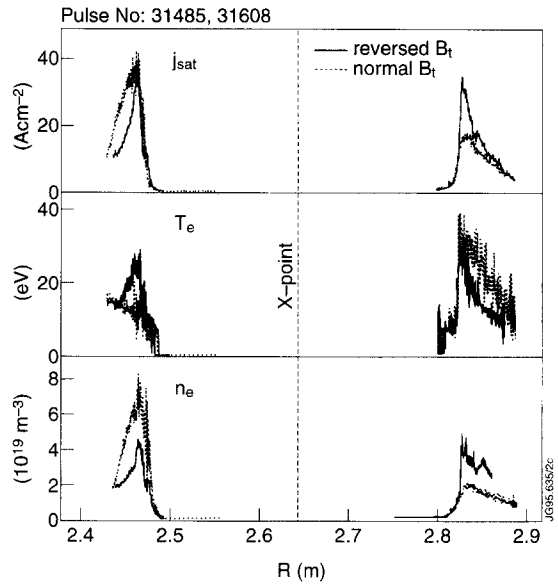

Fig. 5. Profiles of ion saturation current density, electron temperature and density across the target, measured by Langmuir probes in JET.

4.2. Theoretical considerations

There have been a number of attempts to relate observed shifts in the in–out asymmetries caused by the field reversal, with the effect of classical drifts [25,45–48,18,34–36,38,8]. Staebler [49] recently demonstrated that large asymmetries can be spontaneously (following a small initial perturbation) generated due to radiation and/or passage of parallel currents in the scrape-off layer.

Poloidal $\mathbf{E} \times \mathbf{B}$ drift, caused by the radial electric field, drives the plasma towards the outer side in the normal and inner side — in the reversed B_t configuration. Convective power flux associated with this drift is, therefore, in the right direction to explain changes in target power asymmetries [35]. This drift, however, should cause profound changes in poloidal pressure/density distribution which are NOT supported by the experiment. Influence of the poloidal $\mathbf{E} \times \mathbf{B}$ drift on the SOL structure has been first analyzed by Tendler and Rozhansky [45] and later in [18,48]. This drift introduces an extra flux of parallel momentum in the perpendicular direction within the magnetic surface, accounted for by $nmV_\parallel V_\perp$ components of the tensor $nm\mathbf{VV}$ (Eq. (1)). The sum of parallel components of Eq. (1) for ions and electrons in the simplest case of cylindrical geometry and isotropic pressure can then be written as

$$\frac{\partial}{\partial s_\parallel}\left(p + nmV_\parallel^2\right) + \frac{\partial}{\partial s_\perp}\left(nmV_\parallel V_\perp\right) = 0. \qquad (16)$$

Here $p = p_e + p_i$ and m is ion mass. Derivatives over both

parallel and perpendicular coordinates can be replaced by the derivative over the poloidal angle using: $\partial/\partial s_{\|} = B_\theta/B \cdot \partial/r\partial\theta$, $\partial/\partial s_{\perp} \approx \partial/r\partial\theta$. This leads to the following conservation equation:

$$p + nmV_{\|}^2 + nmV_{\|}V_E = const(\theta), \tag{17}$$

where $V_E = \pm E_r/B_\theta$ and positive velocities (both parallel and perpendicular) are assumed to be directed from the outer to the inner side (see $V_{\|}$ in Fig. 1). Therefore, the sign of V_E is negative for normal B_t direction (poloidal $\mathbf{E}\times\mathbf{B}$ drift is directed towards the outer target) and positive for reversed B_t direction. Diamagnetic flux's contribution to Eq. (17) is neglected as it is almost completely divergence-free, as discussed in Section 2.1.

Eliminating $V_{\|}$ and $V_E \equiv M_E c_s$ in Eq. (17) by using boundary conditions (Eq. (11)) and replacing nmc_s^2 with pressure p, the in–out pressure asymmetry can be obtained:

$$\frac{p_{in}}{p_{out}} = \frac{2 + M_{E,out}}{2 - M_{E,in}}. \tag{18}$$

The pressure asymmetry between the strike zones causes plasma flow along the field lines from high to low pressure side giving rise to a net toroidal velocity of the order of E_r/B_θ [45,18]. Thus, instead of the poloidal rotation, the poloidal $\mathbf{E}\times\mathbf{B}$ drift (which, in fact, is in the direction perpendicular to $\mathbf{B}$) generates toroidal momentum and pressure asymmetry between the strike zones. The direction of the toroidal velocity is always along the main plasma current direction, irrespective of the toroidal field direction. In Ref. [50] it is argued that toroidal rotation in the same direction can also be driven near the separatrix by anomalous radial transport in the presence of shear of the poloidal rotation.

For normal B_t direction (M_E negative), according to Eq. (18), $p_{in}/p_{out} < 1$ and for reversed B_t direction (M_E positive) $p_{in}/p_{out} < 1$. Since the power flux, associated with the poloidal $\mathbf{E}\times\mathbf{B}$ drift, is convective, it must be the density asymmetry (not temperature!) that is primarily affected by this drift. The sign of this density asymmetry (as well as associated asymmetries in P_{rad} and H_α) is, however, opposite to the one observed in the experiment. Moreover, the inevitable losses of power due to local hydrogen recycling and impurity radiation (both increase with increase of density) should reduce electron temperature at the side to which the plasma is driven by the poloidal $\mathbf{E}\times\mathbf{B}$ drift and the expected effect on the T_e asymmetry is again opposite to the experimental trend. Regarding experimental pressure asymmetry, no significant changes were detected in Alcator C-Mod [35], while electron pressure asymmetry in favour of the ion drift side (i.e., against the expected effect of the poloidal $\mathbf{E}\times\mathbf{B}$ drift) was observed in JET [51]. Thus, except for the target power asymmetries, the poloidal $\mathbf{E}\times\mathbf{B}$ drift alone would predict changes in all other important asymmetries which are against the experimental trends.

The drift which is in the right direction to explain the n_e, T_e, P_{rad} and H_α asymmetries, is the *radial* $\mathbf{E}\times\mathbf{B}$ drift (see Fig. 1), as was first pointed out by Hinton and Staebler [25]. According to the analysis performed in Ref. [48], radial $\mathbf{E}\times\mathbf{B}$ drift should dominate over the poloidal $\mathbf{E}\times\mathbf{B}$ drift in determining the overall flux pattern in high recycling plasmas. It brings more plasma particles to the inner strike zone in normal B_t discharges and to the outer strike zone — in reversed B_t discharges. Due to the viscous drag experienced by the return parallel flow along the SOL which is induced by the radial drift fluxes, radial $\mathbf{E}\times\mathbf{B}$ drift also causes pressure imbalance between the targets, but of the opposite sign compared to the poloidal drift. The increased density at the divertor to which radial $\mathbf{E}\times\mathbf{B}$ drift supplies particles, increases hydrogenic recycling energy losses, as well as the impurity radiation. This causes the temperature drop and further increase in radiation losses associated with low temperatures (for low Z impurities). The temperature drop causes further increase density owing to the tendency for pressure equilibration (see eqs. (73), (74) of Ref. [48]), thereby providing a positive feedback.

The dependence of electron temperature asymmetry on the B_t direction seems to provide the strongest evidence in favour of the radial $\mathbf{E}\times\mathbf{B}$ drift. The direction of the convective power flow carried by this drift, however, makes it more difficult to explain the experiment. Consistent explanation of the asymmetries through the radial $\mathbf{E}\times\mathbf{B}$ drift can only be achieved if local radiation power losses near the strike zone to which the plasma is driven by the drift, is larger than the convective power flow to it. Whether this is the case can only be established by the detailed 2D code calculations which include drifts.

An explanation for the observed power asymmetries through the poloidal diamagnetic energy flux $\mathbf{q} \sim \mathbf{B}\times\nabla_r T$, was offered in [47,34]. When the radial ion temperature gradient $\nabla_r T_i$ is steeper than $\nabla_r T_e$, as was observed in ASDEX Upgrade and often observed on other machines, the poloidal energy flux is directed towards the outer target in normal and towards the inner target — in reversed B_t plasmas, in agreement with the shifts in the measured asymmetries of power conducted to the target. This explanation, however, is founded on the erroneous assumption that the poloidal diamagnetic flows reach the surface of the target. This is not the case, as was pointed out in Section 3. The diamagnetic flows, after reaching the entrance to the mps, cross through the magnetic pre-sheath in the direction normal to the magnetic surfaces and then continue 'poloidally' on private magnetic surfaces. They do not reach the target and therefore cannot affect in–out power and particle flux asymmetries.

Radial and poloidal $\mathbf{E}\times\mathbf{B}$ drifts seem to be unable to explain the rather symmetric power distribution between the targets in normal B_t configuration at low densities in

JT-60U [30] (see Fig. 2) and hot ion mode regimes in JET (see, for example, Ref. [52]), or even the inner target receiving larger heat flux than the outer one [53,28]. A number of other examples of similar behavior of power and density asymmetries is presented in Ref. [36]. Low density and/or high power discharges present significant challenge for the explanation of divertor asymmetries. Indeed, the SOL plasma in these conditions is relatively 'hot' and poloidal asymmetries in T_e should be rather small, thus reducing the effect of the radial and increasing the effect of the poloidal $\mathbf{E}\times\mathbf{B}$ drift. The latter increases plasma pressure (hence, also power to the target) at the outer side in normal B_t configuration. This is not what is observed in the experiment. To explain the discrepancy, an extra force is needed which would compress the plasma at the inner side. A candidate for such a force — the influence of edge toroidal momentum in the direction of the main plasma current on divertor asymmetries — was suggested in Ref. [54]. In the experiments reviewed in Ref. [54], the toroidal momentum was largest in low density plasmas. To qualitatively explain the experimental data, the toroidal momentum has to be introduced into the model as an *external* boundary condition on the parallel velocity at the separatrix. The toroidal momentum which originates in the SOL due to the pressure asymmetry caused by the poloidal $\mathbf{E}\times\mathbf{B}$ drift, discussed above, cannot perform this role since it intrinsically requires higher plasma pressure at the *outer* side in normal B_t discharges, opposite to experimental observations.

Higher power to the inner target in low density reversed B_t discharges in JT-60U shown on Fig. 2, can naturally be explained by the poloidal $\mathbf{E}\times\mathbf{B}$ drift which drives the plasma to the inner side. The toroidal momentum should be weaker in the reversed B_t, since in the field reversal experiments in JT-60U (also in JET) the toroidal field and plasma current were reversed simultaneously, so that counter-injection was applied in the reversed, whereas co-injection – in normal B_t discharges. It has to be noted, however, that the assumption that the drift (in this case, the poloidal $\mathbf{E}\times\mathbf{B}$ drift) which drives the plasma towards one particular target, increases the power flow to this target, is only valid in low density 'isothermal' (no poloidal variation of temperature) plasmas. In high density plasmas, as discussed above, the increased local radiation has to be taken into account and no simple conclusions on whether the drift towards the target can increase power flow towards this target, can be made.

As was pointed out in Section 4.1, there exists convincing evidence for a much weaker effect of the field reversal on divertor asymmetries at very high densities, when the plasma in the scrape-off layer is rather 'cold'. Such a trend can be explained from the scaling $\rho_{s\theta}/\lambda_{SOL}$ which reflects the role of drifts in the SOL transport (Section 2.2). There was, however, no explanation given so far for lower density limit in conditions close to plasma detachment in reversed field configuration compared to the normal one (there is evidence from JET that reversed B_t plasmas do not necessarily have larger impurity content and radiation power loss, so that earlier disruption can not be easily explained by 'power starvation' of the edge plasma and some other explanation has to be found).

5. Electric currents in the SOL

Experimental and theoretical aspects of divertor bias experiments have recently been reviewed by Staebler [55]. The focus here will be on the contribution of *classical drifts* to the electric current. There can be two main classical contributions to the radial current: one due to the distribution of pressure and parallel convectional energy flux over the magnetic surface (these terms will be referred to as pressure-related terms) and another — due to ion-neutral collisions.

5.1. Currents due to pressure-related terms

Radial current density can be obtained by multiplying Eq. (3) by an electric charge e and summing up ion and electron components. The ion and electron components of the $\mathbf{E}\times\mathbf{B}$ drift and fluxes due to their mutual friction force $\mathbf{R}_{ie}\equiv-\mathbf{R}_{ei}$ will cancel each other out and the result will be

$$\mathbf{j}=j_{\|}\frac{\mathbf{B}}{B}+\frac{1}{B^2}\mathbf{B}\times\nabla p_{\perp}+\frac{\left(p_{\|}-p_{\perp}+nmV_{\|}^2\right)}{B^3}\mathbf{B}\times\mathbf{B}\cdot\nabla\left(\frac{\mathbf{B}}{B}\right). \tag{19}$$

As opposed to equations in Section 3, $p_{\|}$ and $p_{\perp}$ are now assumed to be total (ion plus electron) pressures.

Provided the pressure is isotropic and constant along the field lines and parallel velocity is small (which is usually the case in the plasma core), the only perpendicular current following from Eq. (19) is the current within the magnetic surface perpendicular to the magnetic field, accounted for by the second term on the rhs. In the torus this current, which itself is not constant along the magnetic surface due to $\nabla_r p/B\sim R$ does not satisfy the continuity equation and must be supplemented by parallel Pfirsh–Schlüter current of magnitude (see, for example, Ref. [56], p. 73)

$$j_{\|}=2q\sin\theta\times\nabla_r p/B, \tag{20}$$

where q is the safety factor. This current consists of opposite parallel flows of ions and electrons, proportional to their radial pressure gradients. Its direction, projected onto the poloidal cross-section, is from the bottom to the top of the torus along the magnetic surface for normal and from the top to the bottom — for reversed B_t configuration. The contribution of the ion part of this current (ion parallel flow) to the overall flux pattern in the scrape-off

layer of DITE (in limiter configuration) has been experimentally identified by Hugill [57] from analysis of Langmuir probe data.

On open field lines significant pressure gradients along the magnetic surface can result in non-zero surface averaged radial current. This current was first analyzed by Rozhansky and Tendler [58,59] in cylindrical geometry, with neglect of the last term on the rhs of Eq. (19). The main result of this theory was obtained by integrating radial current density

$$j_r = \frac{1}{B}\frac{\partial p}{r\partial\theta} \tag{21}$$

over the magnetic surface from the entrance of the inner mps to the entrance of the outer mps. For small values of M_E the pressure asymmetry between the two sides from Eq. (18) would give for the pressure difference: $\Delta p \approx M_E p$. By writing $p = nmc_s^2$, dividing the integrated current density by the poloidal circumference $2\pi r$ and remembering the definition of M_E, the averaged radial current density would be

$$\langle j_r \rangle \approx E_r \frac{nmc_s}{2\pi r B B_\theta}. \tag{22}$$

Inclusion of anomalous viscosity into the analysis leads to higher radial current required to establish the same pressure asymmetry, introducing coefficient $K > 1$ into the relation Eq. (22) [58,59].

Eq. (22) gives the averaged current density through the main SOL plasma, excluding contributions from magnetic pre-sheaths at the targets. They, however, can be significant [19]. Moreover, since Eq. (21) is in fact an expression for the radial component of the diamagnetic flux, it should give zero *net* radial current through the magnetic surface in *cylindrical* geometry. Recently, Chankin and Stangeby considered net radial current in *toroidal* geometry [60] with inclusion of both pressure dependent terms in Eq. (19) into the analysis. Their numerical results demonstrated very weak dependence of the net radial current on the E_r. The direction of the current is inwards for the normal and outwards – for the reversed B_t configuration. The origin of such a result can be understood from Fig. 6. Due to the plasma sink towards the target plate, an up–down pressure difference is formed, of the order of the pressure itself, $\Delta p \approx p$ (for the low recycling case modelled in Ref. [60]). This generates the total current per unit toroidal length through both inboard and outboard sides of the magnetic surface, $\approx p/B$. The current is directed inwards on the outboard side and outwards — on the inboards side of the torus, as shown on Fig. 6 for the case of normal B_t direction (the directions are opposite for reversed toroidal field). Due to toroidal variations of both the toroidal field B and surface area, the poloidal average of the above current should be $\approx \varepsilon p/B$, where $\varepsilon = r/R$ is the toroidicity. For the surface averaged radial current density one can, therefore, obtain

$$\langle j_r \rangle \approx enc_s \varepsilon \frac{\rho_s}{2\pi r}. \tag{23}$$

This estimate is quite close to numerical results of Ref. [60]. Weak dependence of the current on E_r, obtained in the calculations, confirms the above interpretation that this current is caused by *up–down* pressure asymmetry, which is weakly affected by the poloidal $\mathbf{E}\times\mathbf{B}$ drift. The latter influences mainly *in–out* asymmetries. For cylindrical geometry ($\varepsilon = 0$), $\langle j_r \rangle = 0$ was found in the calculations [60], as expected.

Estimate (Eq. (23)) is only valid in the main SOL. Closer to the separatrix, poloidal pressure distribution becomes more uniform and large parallel velocities are eliminated. Also, viscous forces must become important due to the large shear of the poloidal rotation near the separatrix. The flux surface average radial current must be zero at the separatrix flux surface. Radial divergence of the radial current, $d\langle j_r \rangle/dr$, should, therefore, create two distinct regions of current flow to the target plates. Near the separatrix, current to the target should be positive for normal and negative — for reversed B_t plasmas. Further away from the separatrix, on the assumption of pressure exponential decay, negative parallel current should flow to the target in normal and positive — in reversed B_t configuration. Some details of the profiles of current flow towards the target in divertor magnetic configuration are discussed in Section 6.

Pressure up–down asymmetry creates vertical electric field and, therefore, radial $\mathbf{E}\times\mathbf{B}$ drift. This ambipolar flow cancels electron component of the pressure-related current [60], so that the current (Eq. (23)) is actually carried only by ions. The dependence of the direction of this current on the toroidal field direction then implies that better particle confinement in the SOL should be expected in normal compared to the reversed B_t case. This effect was proposed in Ref. [60] as part of an explanation for lower power threshold power for the L–H transition in normal B_t configuration (see, for example, Refs. [61,62]).

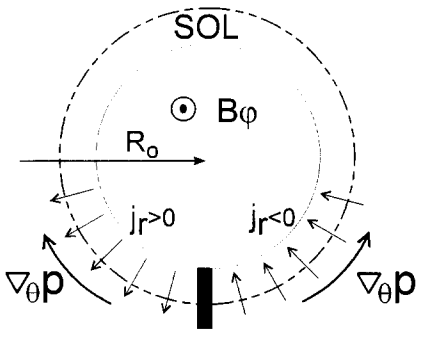

Fig. 6. Directions of radial current density caused by the pressure drop towards the target, on the inboard and outboard parts of the magnetic surface, for the case of normal B_t. For the reversed B_t direction these directions reverse.

By employing up–down asymmetries plus the toroidal effects of higher area and lower magnetic field on the outboard side, to get non-zero radial flows, the above explanation shares the same basis with earlier work by Hinton and Tang [63,64] on the dependence of the neoclassical ion heat transport through the separatrix on the B_t direction. The latter is caused by the up–down asymmetry in ion temperature and is expected to be larger in high recycling plasmas.

5.2. The influence of interaction with neutrals

A large number of papers have been dedicated to the influence of ion-neutral collisions on the radial current. Tsui [65] calculated the width of the poloidal velocity shear layer around the separatrix and Lingertat et al. [66] modelled excessive heat flux conducted to the target by non-ambipolar electron flux just outside the separatrix which is caused by the divergence of the radial current. Both models used the same expression for the radial current and offer explanations for certain features of experiments on TEXT [65] and JET [66]. Radial current was obtained effectively by adding the term $\mathbf{R}_{i-n} \times \mathbf{B}/B^2$, which describes the damping of the poloidal rotation due to ion-neutral interactions (mainly charge-exchange), into the rhs of Eq. (19). Other, pressure dependent terms, however, were ignored in both models. With the poloidal friction force given by: $R_{i-n} = nmV_\perp \nu_{i-n}$, where $V_\perp = \pm(1/enB \cdot \mathrm{d}p/\mathrm{d}r - E_r/B)$ ('+' for normal and '−' for reversed B_t, with positive poloidal velocity assumed to be from the outer to inner divertor target, as adopted in Section 3), the radial current density was obtained:

$$j_r = nm|V_\perp|\nu_{i-n}/eB. \tag{24}$$

This current is carried only by ions and is positive, i.e., outward, for both B_t directions (the field reversal changes the sign of R_{i-n} so that $\mathbf{R}_{i-n} \times \mathbf{B}$ does not change). The magnitude of this current, as will be shown in the next section, is substantially less than the one originating due to pressure-related terms. For comparison with results of biasing experiments we introduce the radial conductivity as: $\sigma = \mathrm{d}j_r/\mathrm{d}E_r$. It is equal to

$$\sigma = nm\nu_{i-n}/eB^2. \tag{25}$$

Considerable enhancement of radial conductivity, compared to the above expression, can be achieved when the influence of ion-neutral interactions on pressure-related terms (i.e., poloidal pressure distribution and parallel convectional energy) is taken into account. Ion-neutral interactions thus perform the role of a trigger, with pressure-related terms being responsible for the bulk of the current in the $j_r(E_r)$ dependence. As was first demonstrated by Boozer [67] (see also later paper Ref. [68]) for the core region, when ion-neutral friction force is added to the rhs of Eq. (1), it can be transformed to give the following relation between toroidal friction force and surface averaged radial current density:

$$\frac{\partial}{\partial t}(nmV_\varphi) = \langle j_r \rangle B_\theta - nm\nu_{i-n}V_\varphi. \tag{26}$$

In the regime dominated by neoclassical viscosity rather then ion-neutral friction force, toroidal velocity V_φ should react on the applied radial electric field so as to keep the combination $(V_\varphi - E_r/B_\theta)$ constant, in the steady state conditions. Radial conductivity, therefore, is

$$\sigma = nm\nu_{i-n}/eB_\theta^2, \tag{27}$$

which is larger than the one given by Eq. (25) by the factor of $(B/B_\theta)^2$. In the regime dominated by ion-neutral collisions, Yoshikawa [69] found that the cylindrical result (Eq. (25)) for the radial conductivity must be multiplied by a Pfirsch–Schlüter factor $(1 + 2q^2)$ with q being the safety factor.

Certain similarities in the plasma flux pattern between the core and the SOL, such as the build-up of the toroidal rotation rather than the poloidal one as a response to the externally applied radial electrical field, pose questions as to whether above factors $(B/B_\theta)^2$ or $(1 + 2q^2)$ of the enhancement of the radial conductivity may apply to the result (Eq. (25)) in the scrape-off layer. For example, *local* radial conductivity (away from the mps layers) which follows from the model of Weynants [70] definitely exhibits the enhancement factor $(B/B_\theta)^2$. The contribution of the mps to the radial current, however, has not been included in this work and would reduce it substantially. Generally, straightforward translation of the results obtained in the core, to the SOL region, is not valid due to the interaction between the SOL plasma and the targets. Pressure asymmetry between the strike zones, for example, should lead to the exchange in toroidal momentum between the plasma and the target due to opposite toroidal directions with which the plasma approaches the two strike zones.

5.3. Comparison with experiment

Classical contributions to radial conductivity were compared with experimental results by Lachambre et al. [71]. Experiments were performed on Tokamak de Varennes (TdeV), which is a small machine with minor radius of 0.27 m and typical toroidal field of $B = 1.5$ T. A schematic cross-section of TdeV with plasma biasing electric connections is shown on Fig. 7. Radial plasma current was driven by applying voltage to neutralization plates with respect to the grounded guard limiters. A phenomenological model based on the assumption that the ion mobility is responsible for the radial current was applied to I–V characteristics obtained in density, current and toroidal field scans.

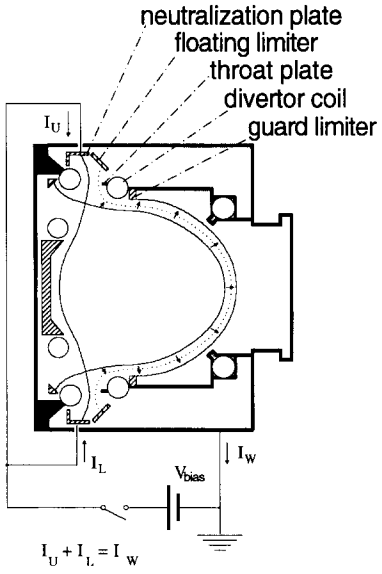

Fig. 7. Schematic cross-section of Tokamak de Varennes with plasma biasing electric connections.

It was found that the best fit to the experimental data from TdeV was a scaling law of the form

$$\sigma \sim n_s^{1.84} I_p^{-1.39}, \tag{28}$$

where n_s is the density at the separatrix. None of the theoretical scaling agrees with such a dependence on plasma parameters. In absolute terms, the dependence (Eq. (22)) falls short of the experimental conductivities by about a factor 5 at low densities and differs even more at high densities. Since the correct expression for the net radial current, which includes mps contributions, Eq. (23), has no dependence on the radial electric field at all, pressure related terms in Eq. (19) cannot provide an explanation for the experiment.

The parametrical dependence of σ in Eq. (28) is closest to the one given by Eq. (27). Both show strong dependence on the plasma current ($I_p \sim rB_\theta$) and density of neutrals, which enters the expression for the collision frequency $\nu_{i-n} = \langle \sigma v_{i-n} \rangle n_n$, was roughly proportional to plasma density in TdeV. However, in absolute value the dependence (Eq. (27)) was found to be short by a factor of about 10 of what is required to explain the experiment, after the neutrals' toroidal acceleration due to plasma toroidal rotation was taken into account. One should also remember that Eq. (27) is likely to overestimate the neutrals' contribution to radial conductivity, as the enhancement factor $(B/B_\theta)^2$ has no justification in the SOL.

Overall, experiments on TdeV provide convincing evidence that at least on this machine radial conductivity has an anomalous nature. More direct experiments (biasing) are needed to extend this conclusion to larger size machines like JET, since the nature of plasma turbulence may strongly depend on the machine/plasma parameters. Alternatively, indirect experimental data such as current profiles to the target plates have to be compared with predictions of models (yet to be developed!) which correctly account for both pressure-related and neutral friction terms and their mutual influence in the SOL, or with the results of 2D numerical codes which include drifts. There is some indirect evidence (see, for example, Refs. [65,66] where comparison between model calculations and experimental data near the separatrix position has been done; see also Section 6 on target current profiles) that classical contributions to radial current may be very important.

6. Profiles of electric current at the divertor target

Electrically conducting divertor target allows for local non-ambipolarity of plasma flow onto its surface. Due to the variety of physical mechanisms that may cause the current flow, fine structure of target profiles of electric current can be rather complicated and difficult to resolve in experiment. Fig. 8 illustrates schematically target current density profiles for the three main mechanisms which were discussed in literature, for both normal and reversed toroidal field directions.

The thermoelectric current (dashed lines on Fig. 8) has been first predicted by Harbour [24] and observed in JET [72]. This current is driven by parallel electric field caused by difference in Debye sheath drops $\approx 3T_e/e$ at the two sides of an open magnetic field line. Another source of parallel current is the electron pressure asymmetry, which can be important when temperatures at the strike zones are nearly equal (full set of equations is given in [73] for the current flow and in [74] for the heat flux to the plates). The target with lower T_e and/or higher p_e receives positive current from the plasma. As was found in experiments in JET [51] and JT-60U [75], the thermoelectric current is almost always parallel to the main plasma current, regardless of the B_t direction. This is due to higher T_e at the outer side in normal B_t plasmas and more equal temperature distribution plus higher pressure at the inner side, or even higher T_e at the inner side — in reversed B_t plasmas. Therefore, considering in–out asymmetries, the thermoelectric current usually flows from the outer to the inner side for normal and from the inner to the outer side – for reversed B_t plasmas. Minor corrections [76] for Eq. (3) in Ref. [51] lead to the following equation for the parallel current density towards the target:

$$j_\parallel = -\frac{\bar{\sigma}_\parallel T_A}{eL_\parallel}\left\{k'\left(\frac{T_B}{T_A}-1\right) - \frac{1}{T_A}\int_A^B \frac{\nabla_\parallel p_e}{n_e} + \ln\left[\frac{1+j_\parallel/j_{sA}}{(1-j_\parallel/j_{sA})^{T_B/T_A}}\right]\right\}. \tag{29}$$

In this equation side A is assumed to have lower electron

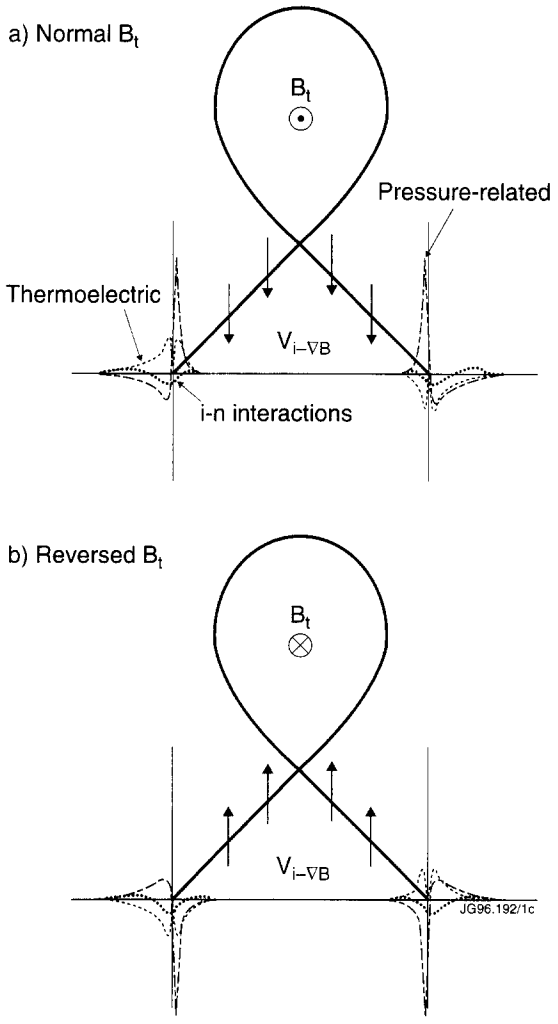

Fig. 8. Schematic illustration of target current density profiles due to the thermoelectric current (dashed lines), radial divergence of currents caused by ion-neutral interactions (dotted lines) and pressure-related terms (dash–dotted lines) for normal (a) and reversed (b) B_t directions.

temperature, $T_A < T_B$, j_s is parallel ion saturation current density to the target plate, $k' \equiv (k + 0.85 - \alpha) \approx 4$, $k \equiv (1/2)\ln(2m_i/\pi m_e)$, $L_\parallel$ – connection length between the two strike zones and inverse averaged parallel resistivity is defined as

$$\overline{\sigma}_\parallel = \frac{e^2 \lambda_{11} L_\parallel}{m_e} \left[\int_A^B \mathrm{d}l_\parallel / n_e \tau_{ei} \right]^{-1}. \tag{30}$$

Other symbols are conventional and may be found in Ref. [73]. Around the separatrix position the connection length $L_\parallel$ approaches infinity logarithmically and $j_\parallel \to 0$. This is schematically reflected on Fig. 8 as $|j_\parallel|$ dipping to zero at the separatrix position. Several other mechanisms to drive parallel currents in the SOL were examined in Ref. [77].

There are also two important contributions to the parallel current which arise from the divergence of the surface averaged radial current, $\mathrm{d}\langle j_r \rangle / \mathrm{d}r$. Radial current density due to pressure-related terms far away from the separatrix is given by Eq. (23), while the radial current density due to damping of the poloidal rotation by ion-neutral interaction with the neutrals is given by Eq. (24). It can be demonstrated that in typical conditions the former should be much larger than the latter. Employing the scaling for the poloidal/perpendicular velocity: $V_\perp \approx c_s \rho_s / \lambda_{sol}$, the current due to ion-neutral interactions can be expressed as

$$j_r|_{i-n} \approx en\rho_s^2 \nu_{i-n} / \lambda_{sol}. \tag{31}$$

The scaling for the ratio of the two currents is

$$\frac{j_r|_{i-n}}{j_r|_p} \approx \frac{2\pi \rho_s \nu_{i-n} r}{\varepsilon \lambda_{sol} c_s}. \tag{32}$$

Making an upper estimate for the ion-neutral collision frequency as $\nu_{i-n} = c_s / \pi R$ for conditions of strong recycling of neutrals in the scrape-off layer (SOL average for ν_{i-n} and c_s is implied), the maximum estimate for the above ratio is $(2/q)(\rho_s / \lambda_{sol})$. Therefore, the current due to the ion-neutral collisions can in typical conditions be neglected compared with the current originating due to pressure-related terms. The radial current caused by ion-neutral collisions is carried by ions and directed away from the separatrix both in the main SOL and in the private region (the poloidal $\mathbf{E} \times \mathbf{B}$ drift has different directions in the main SOL and the private region, as shown on Fig. 1). Its direction does not depend on the direction of the toroidal field. The parallel current to the target, arising from $\mathrm{d}\langle j_r \rangle / \mathrm{d}r$, is shown by dotted lines on Fig. 8. Negative current flows towards the target around the separatrix position and positive current — further away from the separatrix [66].

The pressure-related current, as discussed in the previous section, results from the ion ∇B drift and the up–down asymmetry of plasma pressure. Its direction is inwards for the normal and outwards – for reversed B_t direction. Near the separatrix, current to the target should be positive for normal and negative — for reversed B_t direction. Further away from the separatrix, negative parallel current should flow to the target in normal and positive – in reversed B_t direction. In divertor magnetic configuration with an X-point considerable fraction of the pressure-related current can be continued through the separatrix into the private region and be deposited onto the target just inside the separatrix. Vertical arrows on Fig. 8 show the direction of the ion ∇B drift through the boundary between the divertor SOL and private regions (electron ∇B drift has an opposite direction to the ion one). It is clear that positive charge is flowing into the private region for normal and negative — for reversed B_t configuration. Due to short connection length in the private region this should create narrow peaks of the current density just inside the separatrix. The peaks

should have positive sign for the normal and negative – for the reversed B_t direction. The current density profile caused by pressure-related terms is schematically shown by dash–dotted lines on Fig. 8. The total amount of current flowing into the private region can easily be estimated from guiding center approximation:

$$I \approx en\frac{2(T_i+T_e)}{eBR_0}\times(R_{out}-R_{in})\times 2\pi R_0$$
$$= 4\pi p(R_{out}-R_{in})/B, \quad (33)$$

where R_{in} and R_{out} are major radii of inner and outer separatrix positions at the target.

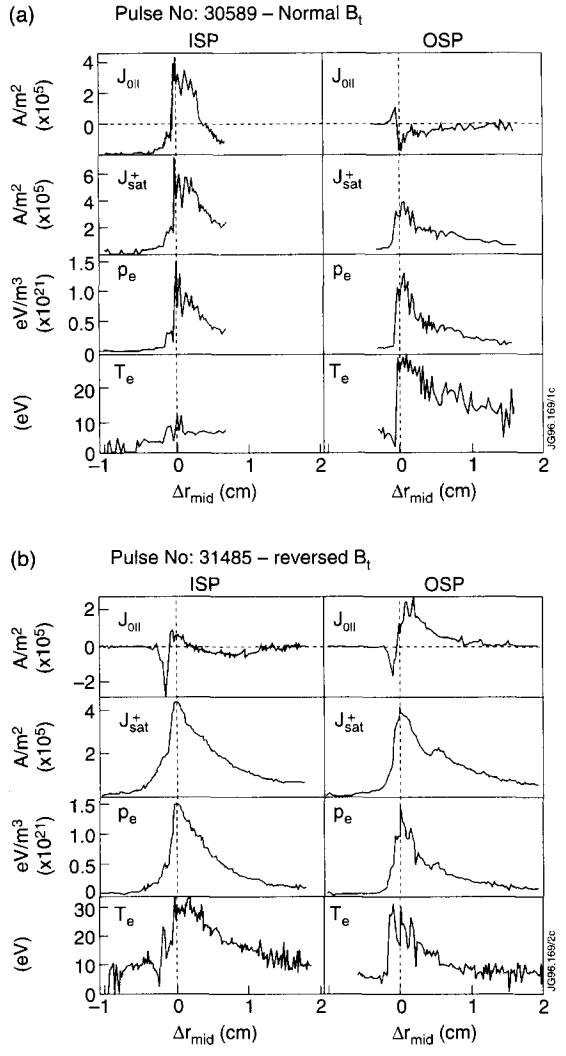

Fig. 9. $j_{o\|}$ profiles for inner strike point (ISP) and outer strike point (OSP) regions for normal and reversed B_t discharges in JET. Also shown are probe-derived profiles of ion saturation parallel current density j^+_{sat}, electron pressure p_e and electron temperature T_e. The profiles are mapped to the outer midplane and plotted as a function of r_{mid}, the midplane radial distance from the separatrix.

Narrow current density peaks inside the private region with opposite signs for normal and reversed B_t have been observed in JET by Schaffer et al. [7]. This paper also gives theoretical treatment of the parallel currents in fluid approximation (all parallel currents originating due to divergence of pressure-related currents are referred to as Pfirsch–Schlüter currents in Ref. [7]). Fig. 9, replicated from Ref. [7], shows current at zero volts measured by Langmuir probes imbedded into the target surface obtained during the horizontal sweep of the X-point for the inner strike point (ISP) and outer strike point (OSP) regions for discharges in both normal and reversed toroidal field. Also profiles of ion saturation current density, electron pressure and electron temperature are shown. The profiles are mapped to the outer midplane and plotted as a function of r_{mid}, the midplane radial distance form the nominal separatrix position. Negative r_{mid} correspond to private region. The position of the separatrix could not be determined with sufficiently high precision and can be slightly different from the one shown on Fig. 9. Narrow current density peaks of opposite signs for the two different field configurations, superimposed on the thermoelectric current can clearly be distinguished on Fig. 9.

7. Conclusions

Classical drifts are expected to make a significant impact on particle, energy and electric current flow pattern in the SOL and divertor. Their incorporation into 2D numerical codes is promising to greatly improve their predictive capacity. Drifts offer potential explanations for a variety of physical phenomena such as poloidal asymmetries, possible extra pinch or outward flow of plasma depending on the B_t direction, non-ambipolarity of radial plasma flow and current flow towards the target.

At present, common understanding among theoreticians is almost reached on the critical issue of modified boundary conditions and a degree of sophistication of the codes is being increased by inclusion of more drift terms. Experimental results on the effects of the toroidal field reversal on divertor asymmetries should provide a proving ground for testing the codes. Present qualitative understanding is insufficient to reliably explain all experimental aspects of these experiments. For example, the n_e, T_e, P_{rad} and H_α asymmetries between the strike zones can be explained by the effect of the radial $\mathbf{E}\times\mathbf{B}$ drift, whereas power to the target asymmetries have their more straightforward explanation through the effect of the poloidal $\mathbf{E}\times\mathbf{B}$ drift. The codes will have to correctly treat drift particle and energy flows, as well as radiative impurity losses and the momentum loss by plasma-neutral interactions, in order to describe the experiment.

The main unresolved issues of the plasma transport related to drifts' implementation into the codes are the absence of knowledge on the contribution of anomalous

radial current and its dependence on the machine/regime parameters (will it be important in ITER, for instance?) and edge toroidal momentum which comes as a (so far, free) boundary parameter for the parallel ion velocity at the separatrix. Apart from the drifts, uncertainty in the poloidal distribution of anomalous transport coefficients, of course, still remains an impediment for increasing predictability of codes. More experimental effort and comparison between measurements and code results is needed to resolve these issues.

Acknowledgements

The author is grateful to P.J. Harbour, I.H. Hutchinson, J.-L. Lachambre, G.F. Matthews, G.J. Radford, M.J. Schaffer and P.C. Stangeby for helpful discussions and critical reading of the manuscript.

References

[1] T.D. Rognlien, J.L. Milovich, M.E. Rensink and G.D. Porter, J. Nucl. Mater. 196–198 (1992) 347.
[2] M. Baelmans, D. Reiter, R.R. Weynants, R. Schneider, J. Nucl. Mater. 220–222 (1995) 982.
[3] G.J. Radford, A.V. Chankin, G. Corrigan, R. Simonini and J. Spence, The Particle and Heat Drift Fluxes and their Implementation into the EDGE2D Transport Code, 5th Plasma Edge Theory Meet., Asilomar, USA, 4–6 Dec. (1995).
[4] M. Baelmans and D. Reiter, New Developments in Plasma Edge Modelling with Particular Emphasis on Drift Flows and Electric Fields, 5th Plasma Edge Theory Meet., Asilomar, USA, 4–6 Dec. (1995).
[5] S.I. Braginskii, in: Reviews of Plasma Physics, ed. M.A. Leontovich, Vol.1 (Consultants Bureau, New York, 1965) p. 205.
[6] G. Chew, M. Goldberger and M. Low, Proc. R. Soc. A 236 (1956) 112.
[7] M.J. Schaffer, A.V. Chankin, H.-Y. Guo, G.F. Matthews and R. Monk, Nucl. Fusion, in press, JET-P(96)11.
[8] A.V. Chankin, D.J. Campbell, S. Clement et al., Plasma Phys. Control. Fusion 38 (1996) 1579.
[9] P.C. Stangeby and G.M. McCracken, Nucl. Fusion 30 (1990) 1225.
[10] K. McCormick, G. Kyriakakis, J. Neuhauser et al., J. Nucl. Mater. 196–198 (1992) 264.
[11] K. McCormick, S. Fiedler, G. Kyriakakis et al., in: 1993 Proc. 20th Eur. Conf. on Control. Fusion and Plasma Phys., Lisbon, Vol. 17C, Part 2 (1993) p. 587.
[12] G.F. Matthews, J. Nucl. Mater. 220–222 (1995) 104.
[13] R. Chodura, Phys. Fluids 25 (1982) 1628.
[14] K.-U. Riemann, Phys. Plasmas 1 (1994) 552.
[15] D. Bohm, in: The Characteristics of Electrical Discharges in Magnetic Fields, eds. A. Guthrie and R.K. Wakerling (McGraw-Hill, New York, 1949) ch. 3, p. 90.
[16] P.C. Stangeby and A.V. Chankin, Phys. Plasmas 2 (1995) 707.
[17] I.H. Hutchinson, Phys. Plasmas 3 (1996) 6.
[18] R.H. Cohen and D.D. Ryutov, Comments Plasma Phys. Control. Fusion 16 (1995) 255.
[19] A.V. Chankin and P.C. Stangeby, Plasma Phys. Control. Fusion 36 (1994) 1485.
[20] H.A. Claaßen and H. Gerhauser, Generalized Bohm's Criterion for Thermal Ions in Oblique Magnetic and Electric Fields, 5th Plasma Edge Theory Meet., Asilomar, USA, 4–6 Dec. (1995).
[21] H.A. Claaßen and H. Gerhauser, Ion Gyro-Cooling in the Magnetic Presheath, 5th Plasma Edge Theory Meet., Asilomar, USA, 4–6 Dec. (1995).
[22] R.H. Cohen and D.D. Ryutov, Phys. Plasma 2 (1995) 2011.
[23] M. Keilhacker, R. Simonini, A. Taroni and M.L. Watkins, Nucl. Fusion 31 (1991) 535.
[24] P.J. Harbour, Contrib. Plasma Phys. 28, Vol. 4–5 (1988) 417.
[25] F.L. Hinton and G.M. Staebler, Nucl. Fusion 29 (1989) 405.
[26] I. Nakazava, T. Shoji and H. Aikawa, in: Proc. 16th Eur. Conf. on Control. Fusion and Plasma Phys., Venice, Vol. 13B, Part 3 (1989) p. 887.
[27] R. Reichle, S. Clement, N. Gottardi, et al., in: Proc. 18th Eur. Conf. on Control. Fusion and Plasma Phys., Berlin (1991) p. 105.
[28] G. Janeschitz, M. Lesourd, J. Lingertat and G. Vlases, in: Proc. 20th Eur. Conf. on Controlled Fusion and Plasma Phys., Lisbon, Vol. 17C, Part 2 (1993) p. 559.
[29] K. Itami, M. Shimada and N. Hosogane, J. Nucl. Mater. 196–198 (1992) 755.
[30] N. Asakura, N. Hosogane, K. Itami, et al., in: Proc. 15th Int. Conf. Plasma Phys. and Controlled Fusion Res. Seville, Sept. 26 to Oct. 1, Spain, Vol. 1 (1994) p. 515.
[31] D.N. Hill, et al., J. Nucl. Mater. 176&177 (1990) 158.
[32] A.W. Leonard C.J. Lasnier J.W. Cuthbertson, et al., J. Nucl. Mater. 220–222 (1995) 325.
[33] A. Herrmann, W. Junker, K. Günther et al., in: Proc. 20th Eur. Conf. on Control. Fusion and Plasma Phys., Lisbon, Vol. 17C, Part 2 (1993) p. 567.
[34] A. Herrmann, W. Junker, K. Günther et al., Plasma Phys. Control. Fusion (1995) 17.
[35] I.H. Hutchinson, B. LaBombard, J.A. Goetz, et al., Plasma Phys. Control. Fusion 37 (1995) 1389.
[36] A.V. Chankin, S. Clement, S.K. Erents, et al., Plasma Phys. Control. Fusion 36 (1994) 1853.
[37] N. Asakura, K. Itami, N. Hosogane, et al., J. Nucl. Mater. 220–222 (1995) 395.
[38] A.V. Chankin, D.J. Campbell, S. Clement, et al., in: Proc. 22nd Eur. Conf. on Control. Fusion and Plasma Phys., Bournemouth, Vol. 19C, Part 3 (1995) p. 289.
[39] M. Laux, A. Herrmann, A. Neu, et al., in: Proc. 22nd Eur. Conf. on Control. Fusion and Plasma Phys., Bournemouth, Vol. 19C, Part 3 (1995) p. 97.
[40] N. Asakura, K. Itami, N. Hosogane, et al., J. Nucl. Mater. 220–222 (1995) 395.
[41] N. Asakura N. Hosogane, Tsuji-Iio, et al., Nucl. Fusion 36 (1996) 795.
[42] D.J. Campbell and the JET Team, in: 15th Int. Conf. on Plasma Phys. and Control. Fusion Res. Seville, Sept. 26 to Oct. 1, Spain, Vol. 1 (1994) p. 527.
[43] V. Mertens, W. Junker, M. Laux, et al., Plasma Phys. Control. Fusion 36 (1994) 1307.
[44] R.D. Monk, D.J. Campbell, S. Clement, et al., in: Proc. 22nd

Eur. Conf. on Control. Fusion and Plasma Phys., Bournemouth, Vol. 19C, Part 3 (1995) p. 293.
[45] M. Tendler and V. Rozhansky, Comments Plasma Phys. Control. Fusion 13 (1990) 191.
[46] S.I. Krasheninnikov, D.J. Sigmar and P.N. Yushmanov, Phys. Plasmas 2 (1995) 1972.
[47] M. Kaufmann, H.-S. Bosch, A. Field et al., Plasma Phys. Control. Fusion 35 (1993) B205.
[48] P.C. Stangeby and A.V. Chankin, Nucl. Fusion 36 (1996) 839.
[49] G.M. Staebler, Nucl. Fusion, in press, GA-A22053 (1995).
[50] M. Tendler and V. Rozhansky, J. Nucl. Mater. 196–198 (1992) 912.
[51] A.V. Chankin, S. Clement, L. de Kock, et al., J. Nucl. Mater. 196–198 (1992) 739.
[52] S. Clement, D.J. Campbell, A.V. Chankin, et al., in: Proc. 22nd Eur. Conf. on Control. Fusion and Plasma Phys., Bournemouth, Vol. 19C, Part 3 (1995) p. 309.
[53] K. Itami, T. Fukuda, Y. Ikeda, et al., J. Nucl. Mater. 176&177 (1990) 504.
[54] A.V. Chankin and W. Kerner, Nucl. Fusion 36 (1996) 563.
[55] G.M. Staebler, J. Nucl. Mater. 220–222 (1995) 158.
[56] B.B. Kadomtsev and O.P. Pogutse, Nucl. Fusion 11 (1971) 67.
[57] J. Hugill, J. Nucl. Mater. 196–198 (1992) 918.
[58] V. Rozhansky and M. Tendler, in: Proc. 20th Eur. Conf. on Control. Fusion and Plasma Physics, Lisbon, Vol. 17C, Part 2 (1993) p. 843.
[59] V. Rozhansky and M. Tendler, Phys. Plasma 1 (1994) 2711.
[60] A.V. Chankin and P.C. Stangeby, Plasma Phys. Control. Fusion, 38 (1996) 1879.
[61] F. Wagner, R. Bartiromo, G. Becker, et al., Nucl. Fusion 25 (1985) 1490.
[62] D. Ward, V. Bhatnagar, M. Bures, et al., in: Proc. 18th Eur. Conf. on Control. Fusion and Plasma Physics, Berlin, Vol. 15C, Part 1 (1991) p. 353.
[63] F.L. Hinton, Nucl. Fusion 25 (1985) 1457.
[64] W.M. Tang and F.L. Hinton, Nucl. Fusion 28 (1988) 443.
[65] H.Y.W. Tsui, Phys. Fluids B 4 (1992) 4057.
[66] J. Lingertat, K. Günther and A. Loarte, J. Nucl. Mater. 220–222 (1995) 198.
[67] A.H. Boozer, Phys. Fluids 19 (1976) 149.
[68] J. Cornelis, R. Sporken, G. Van Oost and R.R. Weynants, Nucl. Fusion 34 (1994) 171.
[69] S. Yoshikawa, Princeton Plasma Physics Laboratory Report, MATT-346 (1965).
[70] R.R. Weynants, Plasma Phys. Control. Fusion 37 (1995) 63.
[71] J.-L. Lachambre, B. Quirion, C. Boucher, et al., Nucl. Fusion 34 (1994) 1431.
[72] P.J. Harbour, D.D.R. Summers, S. Clement et al., J. Nucl. Mater. 162–164 (1988) 236.
[73] G.M. Staebler and F.L. Hinton, Nucl. Fusion 29 (1989) 1820.
[74] P.C. Stangeby, Nucl. Fusion 30 (1990) 1153.
[75] K. Itami, M. Shimada, N. Asakura, et al., in: Proc. 14th Int. Conf. Plasma Phys. and Control. Fusion Res. Würzburg, Sept. 30 to Oct. 7, Germany, Vol. 1 (1992) p. 391.
[76] P.C. Stangeby, private communication.
[77] M.J. Schaffer and B.J. Leikind, Nucl. Fusion 31 (1991) 1740.